JACS
JOURNAL OF THE AMERICAN CHEMICAL SOCIETY
Communication
pubs.acs.org/JACS

Strong Localization of Anionic Electrons at Interlayer for Electrical and Magnetic Anisotropy in Two-Dimensional Y_2C Electride

Jongho Park,[†,‡,¶] Kimoon Lee,[§,¶] Seung Yong Lee,[†,‡] Chandani N. Nandadasa,[∥] Sungho Kim,[‡] Kyu Hyoung Lee,[⊥] Young Hee Lee,[†,‡] Hideo Hosono,[#] Seong-Gon Kim,[∥] and Sung Wng Kim*[,†]

[†]Department of Energy Science, Sungkyunkwan University (SKKU), Suwon 16419, Republic of Korea
[‡]Center for Integrated Nanostructure Physics, Institute for Basic Science (IBS), Suwon 16419, Republic of Korea
[§]Department of Physics, Kunsan National University, Gunsan 54150, Republic of Korea
[∥]Department of Physics & Astronomy and Center for Computational Sciences, Mississippi State University, Mississippi State, Mississippi 39792, United States
[⊥]Department of Nano Applied Engineering, Kangwon National University, Chuncheon 24341, Republic of Korea
[#]Materials Research Center for Element Strategy, Tokyo Institute of Technology, Yokohama 226-8503, Japan

Supporting Information

ABSTRACT: We have synthesized a single crystalline Y_2C electride of centimeter-scale by floating-zone method and successfully characterized its anisotropic electrical and magnetic properties. In-plane resistivity upturn at low temperature together with anisotropic behavior of negative magnetoresistance is ascribed to the stronger suppression of spin fluctuation along in-plane than that along the *c*-axis, verifying the existence of magnetic moments preferred for the *c*-axis. A superior magnetic moment along the *c*-axis to that along the in-plane direction strongly demonstrates the anisotropic magnetism of Y_2C electride containing a magnetically easy axis. It is clarified from the theoretical calculations that the anisotropic nature of the Y_2C electride originates from strongly localized anionic electrons with an inherent magnetic anisotropy in the interlayer spaces.

Electrides are ionic crystals in which electrons serve as anions.[1,2] Because the anionic electrons are loosely bound to the positively charged lattice framework, the physical and chemical properties derived from the anionic electrons markedly differ from those of typical ionic crystals with interstitial electrons trapped at anion vacancies such as *F*-center and ordinary metals with nearly free electrons. The first room temperature stable inorganic $[Ca_{24}Al_{28}O_{64}]^{4+}\cdot 4e^-$ (C12A7) electride exhibits various electronic phases from an insulating to superconducting state depending on the concentration of anionic electrons in the three-dimensional network of interconnected cages.[3,4] The versatile functionality of the C12A7 electride has been successfully demonstrated in efficient electron-emitting devices and powerful reducing catalytic reactions.[5]

Recently, a new class of two-dimensional (2D) electride of $[Ca_2N]^+\cdot e^-$ has also been reported.[6] On the basis of the highly delocalized nature of anionic electrons confined in 2D space, the $[Ca_2N]^+\cdot e^-$ electride exhibits an extremely high mobility (520 $cm^2 V^{-1} s^{-1}$) even under a dense electron concentration (1.39×10^{22} cm^{-3}).[6] Inspired by this discovery, several kinds of electrides with 2D isostructure have been predicted and synthesized in various material groups including nitride and carbide systems.[7−9] Among the new 2D electrides, the rare earth hypocarbide (RE_2C, where RE is rare earth element) intrigues a new functionality based on anionic electrons such as magnetism.[8,9] Depending on the RE elements, both the degree of localization and the ground state of anionic electrons are expected to be diverse, inducing itinerant ferromagnetic to long-ranged ferromagnetic states.[7,8,10−13] In particular, the Y_2C electride that is composed only of paramagnetic elements is expected to exhibit ferromagnetic instability originating from the anionic electrons, but this is hard to demonstrate in experiments because of the absence of high-quality single crystals that can clarify an intrinsic and anisotropic magnetic property of the 2D layered electride.[9,10] Further, the relation between localization degree of interstitial electrons in 2D space and anisotropic electrical and magnetic properties has not been discussed.

Here, we report the strong localization of anionic electrons at 2D interlayer spacing that is critical for inducing anisotropic electrical and magnetic properties of the Y_2C electride. A high-quality centimeter-scale single crystalline Y_2C electride allows rigorous experimental studies on anisotropic physical properties, which are verified from the spin-polarized density functional theory (DFT) calculations.

Stoichiometric polycrystalline Y_2C ingot rods were used for the single-crystal growth by the floating zone (FZ) melting method. To fabricate a stoichiometric polycrystalline Y_2C ingot rod, we mixed Y metal and graphite chips in a 2:1 molar ratio. The mixed sample was melted using an arc melting furnace under high purity argon atmosphere (Ar = 99.999%). To improve homogeneity of the single-phase Y_2C sample, we repeated the melting process of the ingot at least 3 times. The single crystal was grown by four-mirror FZ melting method with the rod-type ingots under high purity argon (Ar = 99.999%) and pressurized conditions (0.3 MPa) to prevent Y vaporization. The feed and seed rods were rotated at 10 rpm, and the growing speed was 10 mm per hour. For out-of-plane resistivity (ρ_{out}) of the single-crystal Y_2C sample to be measured, electrical contacts in the quasi-four point probe

Received: November 19, 2016
Published: December 27, 2016

DOI: 10.1021/jacs.6b11950
J. Am. Chem. Soc. 2017, 139, 615−618

geometry were made by applying Ag paste onto the samples.[14] For precise measurements of in-plane resistivity (ρ_{in}) under varied magnetic fields (H), we adopted the stamp method, which has Hall bar configurations.[6] Temperature (T)- and magnetic field (H)-dependent electrical and magnetic properties of the single crystalline Y_2C were measured by physical parameter measurement system (PPMS) equipped with a vibrating sample magnetometer (VSM). All manipulations were conducted in a purified Ar-filled glovebox due to the degradation of Y_2C electride under an ambient oxygen and water vapor atmosphere.

For density functional theory (DFT) calculations, total energies were calculated within DFT in the generalized gradient approximation (GGA) with the Perdew–Burke–Ernzerhof (PBE96) functional[15,16] using the projector augmented wave (PAW) method as implemented in VASP.[17] The Y_2C crystal was represented by a primitive rhombohedral unit cell containing one chemical formula, and the plane wave basis set cutoff energy was set to 400 eV. In most calculations, $16 \times 16 \times 16$ sampling of the Brillouin zone was used, whereas $32 \times 32 \times 32$ sampling was used for electron localization function (ELF) and magnetization density map (MDM) calculations. All calculations were spin polarized, and positions of atoms, size, and the shape of the unit cell were fully relaxed to obtain the optimized lattice structure. The crystal structure of the Y_2C electride, which is an anti-$CdCl_2$-type structure with $R\bar{3}m$ space group, is shown in the inset of Figure 1(a). On the basis of the Rietveld refinement of the powder X-ray diffraction (PXRD) pattern, it is revealed that the edge-sharing CY_6 octahedra forms a positively charged layer unit, and each layer unit has a separation of 3.29 Å (Figure S1 and Table S1). Because the layer unit can be regarded as a cationic layer structured framework considering the general chemical formula $[Y^{3+}{}_2C^{4-}]^{2+}$, it is supposed that the anionic electrons of high density are confined between $[Y_2C]^{2+}$ layers as constructing the 2D $[Y_2C]^{2+}\cdot 2e^-$ electride. Panels a and b in Figure 1 show X-ray diffraction (XRD) patterns for the Y_2C single crystal grown by the FZ method. As shown in Figure 1(a and b), the exclusive reflection peaks from (00l) planes and periodic reflections with the degree of 120° are observed for out-of-plane (2θ) and azimuthal in-plane (ϕ) scans, respectively. This indicates that the crystal surface is well oriented to the (003) plane where the 2D space is located in constructing the rhombohedral unit cell of Y_2C with 3-fold symmetry, as confirmed by the PXRD results.

Figure 2(a) shows T dependence of ρ_{in} and ρ_{out} for a bulky single crystal of the Y_2C electride. The metallic transports with

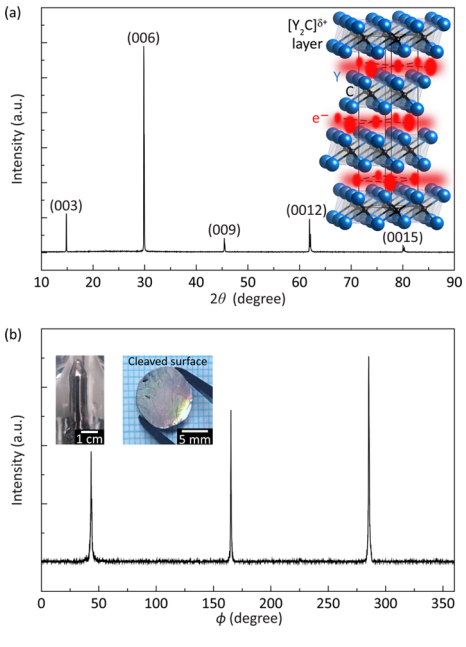

Figure 1. Structural characterizations of single-crystalline Y_2C electride. X-ray diffraction patterns measured by Cu Kα radiation for the Y_2C single crystal. (a) 2θ scan for the cleaved surface of the Y_2C single crystal. The inset schematic illustrates the crystal structure of Y_2C electride containing interstitial electrons between $[Y_2C]^{\delta+}$ layers. (b) The ϕ scan for the cleavage surface of the Y_2C single crystal. Inset photos display the single crystal rod grown by FZ melting method (left) and cleaved surface of single-crystalline Y_2C electride (right).

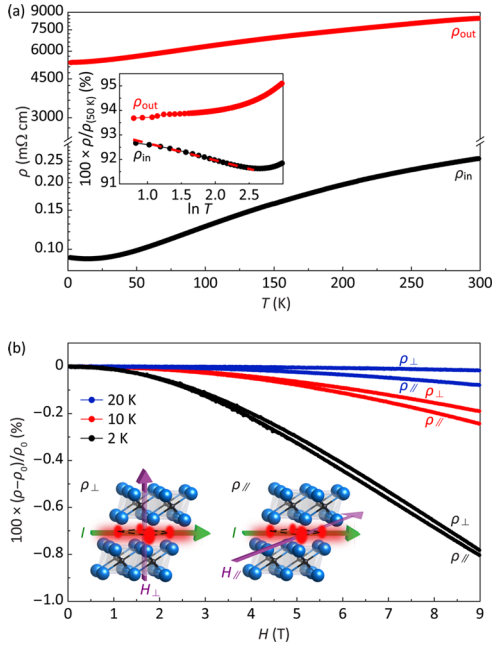

Figure 2. Anisotropic magneto-electrical transport properties of the Y_2C single crystal. (a) Temperature dependence of in-plane (ρ_{in}) and out-of-plane (ρ_{out}) for the Y_2C single crystal. The normalized ρ_{in} and ρ_{out} below 50 K are displayed in the inset. (b) Magnetic field dependence of resistance under different T and H directions for the Y_2C single crystal. Inset schematics provide an illustration of the geometry for magneto-resistance measurements.

positive T dependences are observed in both directions, whereas the ρ values in two directions show a clear difference over the temperature range of 2–300 K with a high anisotropy ratio (ρ_{out}/ρ_{in}) of 5.8×10^4 at 2 K. This indicates that the electrical conduction along the (00l) plane is less suppressed from electron–phonon scattering compared to that perpendicular to the (00l) plane.[6,18] In a low T range (inset, Figure 2(a)), ρ_{in} exhibits ln T dependence, showing increasing behavior below the critical temperature (T_c) of 15 K, whereas ρ_{out} continuously decreases as T decreases. This indicates that the interaction of conduction electrons with spin moment exists along the in-plane direction parallel to the (00l) plane even in the absence of magnetic elements as spin-aligned scattering sources.[3,19] The magnetoresistance (MR) is examined along the (00l) plane with respect to the direction of applied magnetic field (H) to clarify the detailed scattering mechanism, as depicted in the inset of Figure 2(b). In both directions of out-of-plane perpendicular ($\Delta\rho_\perp(H) = \rho_\perp(H) - \rho_\perp(0)$) and in-plane transverse ($\Delta\rho_\parallel(H) = \rho_\parallel(H) - \rho_\parallel(0)$) to the (00$l$) plane, negative MRs are observed. This is in contrast to the MR behavior of the Ca_2N electride in

DOI: 10.1021/jacs.6b11950
J. Am. Chem. Soc. 2017, 139, 615–618

which $\Delta\rho_{\perp}(H)$ and $\Delta\rho_{\parallel}(H)$ showed anisotropy with opposite sign due to the diffusive 2D transport of delocalized anionic electrons along the (00l) plane.[6] Because the carrier mobility of Y_2C (5.6 $cm^2 V^{-1} s^{-1}$ at 2 K) is much smaller than that of Ca_2N (520 $cm^2 V^{-1} s^{-1}$ at 2 K) (Figure S2), it is reasonable to suppose that the anionic electrons of Y_2C are more strongly localized than those of Ca_2N. Further, from the negative MR in both $\Delta\rho_{\perp}(H)$ and $\Delta\rho_{\parallel}(H)$ that is a characteristic feature of a system with weak localization or well-aligned spin, the negative MR of Y_2C in both directions is attributed to the suppression of spin fluctuation as typical ferromagnetic metals, not the weak localization.[20,21] It should be noted, however, that the Y_2C electride is composed of only paramagnetic elements yttrium and carbon. Moreover, dissimilar MR with the same negative sign is often shown in magnetocrystalline materials with highly anisotropic structure containing easy and hard axes for the magnetization.[22,23] As observed from the ferromagnetic single crystal with structural anisotropy, such as Gd, the magnitude of MR for applied H along the hard axis is superior to that along the easy axis where the anisotropic energy is minimized.[22] These results strongly indicate that the Y_2C electride contains an inherent magnetic constituent with anisotropic geometry, leading to the anisotropic magnetoelectrical transport governed by spin-associated scattering.

To confirm the anisotropy of the Y_2C electride, we measured the magnetization (M) under different H directions. Figure 3(a)

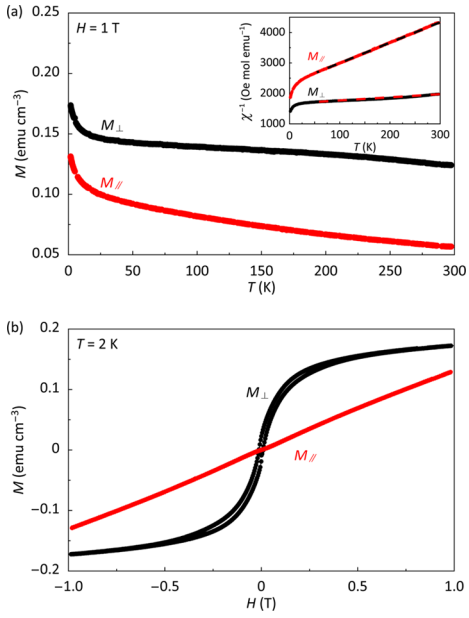

Figure 3. Anisotropic magnetic properties of the Y_2C single crystal. (a) Temperature dependence of magnetizations (M) under an applied magnetic field (H) of 1 T perpendicular ($M_{\perp}$) and parallel ($M_{\parallel}$) to the (00l) plane of the single-crystalline Y_2C electride. Inset shows χ^{-1} versus T curves in both directions under H = 1 T. Dashed lines are Curie law fittings for calculations of μ_{eff}. (b) M versus H curves depending on the direction of applied H at T = 2 K, clearly showing anisotropy.

shows M curves as a function of T for the Y_2C single crystal under H along the c-axis and ab-plane, denoted as $M_{\perp}$ and $M_{\parallel}$, respectively. $M_{\perp}$ and $M_{\parallel}$ are measured under H of 1 T. On the basis of the Curie law (dashed line in the inset of Figure 3(a), the effective magnetic moments (μ_{eff}) are calculated as 2.82 μ_B and 1.08 μ_B (μ_B: Bohr magneton) per unit cell for $M_{\perp}$ and $M_{\parallel}$, respectively. These results firmly show the anisotropy of the magnetic properties for the Y_2C electride. When we measure M versus H curves in different H directions as shown in Figure 3(b), a relatively large $M_{\perp}$ value with saturation behavior can be obtained, whereas $M_{\parallel}$ shows a gradual and linear increase up to H of 1 T as a typical Pauli paramagnetic metal.[20,24] These results demonstrate that the c-axis of the Y_2C crystal is a magnetically easy axis compared to its perpendicular plane, which is also confirmed by the anisotropic MR results as observed in Figure 2(b). Combining this magnetic anisotropy with the electrical transport anisotropy, it is concluded that the Y_2C electride exhibits anisotropic magnetic properties containing localized moments that tend to align along the c-axis.

To clarify the origin of the anisotropy, we performed spin-polarized DFT calculations for the Y_2C electride. The calculated band structure of each atomic contribution containing an interstitial anionic electron site (denoted as X) is shown in Figure 4(a–c). Unlike the previously reported Ca_2N, where a well-dispersed single band appears across E_F, narrower bands composed of electron and hole pockets are observed near E_F, suggesting a more localized nature of carriers for Y_2C.[6] The bands for spin-up and -down split spontaneously with the energy gain of ΔE_m = 16 meV per formula unit. As displayed in Figure 4(a–c), Y and X mainly contribute to the electrons near E_F, indicating the hybridization states between interstitial electrons and Y orbital. From the calculations of ELF as shown in Figure 4(d and e), a biased value of ELF for the spin-up and -down state is converged on the interstitial site resulting in the peanut-shaped effective ELF (difference of spin-up and -down ELF values) on X as displayed in Figure 4(f). Considering this with the atomic contribution from the band structure, it is strongly convincing that the highly localized anionic electrons occupy the interstitial X sites not on the atomic orbitals with nonzero spin moment. The MDM as depicted in Figure 4(g) also verifies well the peanut-shaped anionic electrons at interstitial X sites and exhibits a nonzero magnetic moment even larger than that from Y atoms showing clear distinction from the delocalized anionic electrons with no magnetization density in Ca_2N (see Figure S3). When we calculate magnetic anisotropy energy from the difference of total energies with the spin quantization in the (100) hard and (001) easy axis, it is obtained as 0.027 eV. As a consequence, the anisotropic transport and magnetism in the Y_2C electride originate from the localized interstitial electrons in 2D space, which are more favorable for aligning along the c-axis more easily. From the successful growth of high-quality single-crystalline Y_2C electride and rigorous examination of anisotropic electrical and magnetic properties, we have found that the interstitial anionic electrons are strongly localized in a 2D interlayer space of the layer-structured Y_2C electride. Distinct differences in electrical transport characteristics (ρ_{out}/ρ_{in} ratio up to 5.8×10^4 at 2 K as well as inferior MR for c-axis) between in-plane and out-of-plane are clearly observed, and superior magnetization along the c-axis compared to that of the in-plane direction is also characterized. Spin-polarized DFT calculations also clarify that such an anisotropic nature of the Y_2C electride originates from strongly localized anionic electrons with an inherent magnetic anisotropy in the interlayer space. We envisage that the RE_2C-type electride can be intriguing with new functionality of highly localized anionic electrons under a low dimensional space, such as exceptional orbital-free magnetism.[25]

DOI: 10.1021/jacs.6b11950
J. Am. Chem. Soc. 2017, 139, 615–618

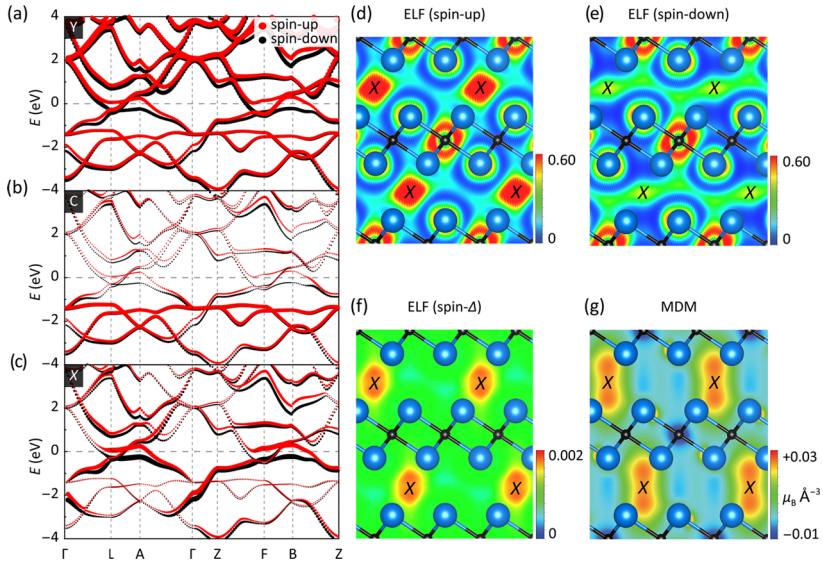

Figure 4. Electronic structure of the Y_2C electride. (a–c) Calculated spin-polarized electronic band structure of the Y_2C electride for each chemical species of Y, C, and interstitial site denoted as *X*, respectively (red: spin-up; black: spin-down). The coordination of the *X*-site is 6c (0, 0, 0.5) with $R\bar{3}m$ space group. Fermi level is set to zero. (d–f) Electron localization function (ELF) for spin-up, spin-down, and difference (Δ) between spin-up and -down, respectively. (g) Magnetic density map (MDM) on the $(\bar{1}10)_R$ plane.

■ ASSOCIATED CONTENT

Supporting Information

The Supporting Information is available free of charge on the ACS Publications website at DOI: 10.1021/jacs.6b11950.

Structural information on the Y_2C electride, powder X-ray diffraction (PXRD) analysis, Rietveld refinement, Hall effect measurement, carrier concentration, electron mobility, and MDM for Ca_2N (PDF)

■ AUTHOR INFORMATION

Corresponding Author

*kimsungwng@skku.edu

ORCID

Sung Wng Kim: 0000-0002-4802-5421

Author Contributions

¶J.P. and K.L. contributed equally to this work.

Notes

The authors declare no competing financial interest.

■ ACKNOWLEDGMENTS

This research was supported by the Creative Materials Discovery Program through the National Research Foundation of Korea (NRF) funded by the Ministry of Science, ICT, and Future Planning (2015M3D1A1070639). It was also partly supported by the World Research Hub Initiative (WRHI) program, Tokyo Tech, and the Center for Computational Science (CCS) at Mississippi State University. Computer time allocation has been provided by the High Performance Computing Collaboratory (HPC2) at Mississippi State University.

■ REFERENCES

(1) Dye, J. L. *Science* **1990**, *247*, 663.
(2) Dye, J. L. *Acc. Chem. Res.* **2009**, *42*, 1564.
(3) Kim, S. W.; Matsuishi, S.; Nomura, T.; Kubota, Y.; Takata, M.; Hayashi, K.; Kamiya, T.; Hirano, M.; Hosono, H. *Nano Lett.* **2007**, *7*, 1138.
(4) Miyakawa, M.; Kim, S. W.; Hirano, M.; Kohama, Y.; Kawaji, H.; Atake, T.; Ikegami, H.; Kono, K.; Hosono, H. *J. Am. Chem. Soc.* **2007**, *129*, 7270.
(5) Kitano, M.; Inoue, Y.; Yamazaki, Y.; Hayashi, F.; Kanbara, S.; Matsuishi, S.; Yokoyama, T.; Kim, S.-W.; Hara, M.; Hosono, H. *Nat. Chem.* **2012**, *4*, 934.
(6) Lee, K.; Kim, S. W.; Toda, Y.; Matsuishi, S.; Hosono, H. *Nature* **2013**, *494*, 336.
(7) Tada, T.; Takemoto, S.; Matsuishi, S.; Hosono, H. *Inorg. Chem.* **2014**, *53*, 10347.
(8) Inoshita, T.; Jeong, S.; Hamada, N.; Hosono, H. *Phys. Rev. X* **2014**, *4*, 031023.
(9) Zhang, X.; Xiao, Z.; Lei, H.; Toda, Y.; Matsuishi, S.; Kamiya, T.; Ueda, S.; Hosono, H. *Chem. Mater.* **2014**, *26*, 6638.
(10) Inoshita, T.; Hamada, N.; Hosono, H. *Phys. Rev. B: Condens. Matter Mater. Phys.* **2015**, *92*, 201109.
(11) Pickard, C. J.; Needs, R. *Phys. Rev. Lett.* **2011**, *107*, 087201.
(12) Dong, S.; Zhao, H. *Appl. Phys. Lett.* **2012**, *100*, 142404.
(13) Dong, S.; Zhao, H. *Phys. Status Solidi B* **2014**, *251*, 527.
(14) Maeno, Y.; Hashimoto, H.; Yoshida, K.; Nishizaki, S.; Fujita, T.; Bednorz, J.; Lichtenberg, F. *Nature* **1994**, *372*, 532.
(15) Blöchl, P. E. *Phys. Rev. B: Condens. Matter Mater. Phys.* **1994**, *50*, 17953.
(16) Perdew, J. P.; Burke, K.; Ernzerhof, M. *Phys. Rev. Lett.* **1996**, *77*, 3865.
(17) Kresse, G.; Furthmüller, J. *Phys. Rev. B: Condens. Matter Mater. Phys.* **1996**, *54*, 169.
(18) Natori, A. *J. Phys. Soc. Jpn.* **1986**, *55*, 4370.
(19) Kondo, J. *Solid State Physics*; Academic Press: New York, 1970.
(20) Blundell, S. *Magnetism in condensed matter*; Oxford University Press, 2001.
(21) Hwang, H. Y.; Cheong, S. W.; Ong, N. P.; Batlogg, B. *Phys. Rev. Lett.* **1996**, *77*, 2041.
(22) Volkenshtein, N.; Dyakina, V. *Soviet Journal of Experimental and Theoretical Physics Letters* **1966**, *4*, 268.
(23) Coleman, R. V.; Morris, R. C.; Sellmyer, D. J. *Phys. Rev. B* **1973**, *8*, 317.
(24) Kittel, C. *Introduction to solid state physics*; Wiley, 2005.
(25) Bernu, B.; Cândido, L.; Ceperley, D. M. *Phys. Rev. Lett.* **2001**, *86*, 870.

DOI: 10.1021/jacs.6b11950
J. Am. Chem. Soc. 2017, 139, 615–618